Biophysical Journal
Article

Biophysical Society

Phosphomimetic substitutions in TDP-43's transiently α-helical region suppress phase separation

Raza Haider,[1] Srinivasa Penumutchu,[2] Solomiia Boyko,[1] and Witold K. Surewicz[1,*]
[1]Department of Physiology and Biophysics, Case Western Reserve University, Cleveland, Ohio and [2]Northeast Ohio High Field NMR Facility, Case Western Reserve University, Cleveland, Ohio

ABSTRACT Phosphorylated TAR DNA-binding protein of 43 kDa (TDP-43) is present within the aggregates of several age-related neurodegenerative disorders, such as amyotrophic lateral sclerosis, frontotemporal lobar degeneration, and Alzheimer's disease, to the point that the presence of phosphorylated TDP-43 is considered a hallmark of some of these diseases. The majority of known TDP-43 phosphorylation sites detected in amyotrophic lateral sclerosis and frontotemporal lobar degeneration patients is located in the low-complexity domain (LCD), the same domain that has been shown to be critical for TDP-43 liquid-liquid phase separation (LLPS). However, the effect of these LCD phosphorylation sites on TDP-43 LLPS has been largely unexplored, and any work that has been done has mainly focused on sites near the C-terminal end of the LCD. Here, we used a phosphomimetic approach to explore the impact of phosphorylation at residues S332 and S333, sites located within the transiently α-helical region of TDP-43 that have been observed to be phosphorylated in disease, on protein LLPS. Our turbidimetry and fluorescence microscopy data demonstrate that these phosphomimetic substitutions greatly suppress LLPS, and solution NMR data strongly suggest that this effect is at least in part due to the loss of α-helical propensity of the phosphomimetic protein variant. We also show that the S332D and S333D substitutions slow TDP-43 LCD droplet aging and fibrillation of the protein. Overall, these findings provide a biophysical basis for understanding the effect of phosphorylation within the transiently α-helical region of TDP-43 LCD on protein LLPS and fibrillation, suggesting that phosphorylation at residues 332 and 333 is not necessarily directly related to the pathogenic process.

SIGNIFICANCE The link between TDP-43 phosphorylation and neurodegenerative disease is well established, as pathognomonic inclusions in diseases such as amyotrophic lateral sclerosis and frontotemporal lobar degeneration are specifically marked by phosphorylated C-terminal fragments of this protein. In this study, we determined how phosphorylation at residues S332 and S333, two sites within the critically important transiently α-helical region that have been identified to be phosphorylated in disease, affects the protein's liquid-liquid phase separation, a phenomenon associated with TDP-43 proteinopathies. The present findings expand our mechanistic understanding of the pathogenic process in these neurodegenerative diseases.

INTRODUCTION

TAR DNA-binding protein of 43 kDa (TDP-43) is a nucleocytoplasmic, nucleic acid-binding protein that has been found in the proteinaceous inclusions that characterize a number of neurodegenerative diseases, including tau-negative, ubiquitin-positive frontotemporal lobar degeneration, amyotrophic lateral sclerosis, cerebral age-related TDP-43 with sclerosis, limbic predominant age-related TDP-43 encephalopathy, and Alzheimer's disease (1–5). Much of the TDP-43 within these inclusions is post-translationally modified, with ubiquitination, N-terminal truncation, and hyperphosphorylation being among the most widely reported (1,2,6,7). Hyperphosphorylated TDP-43, in fact, is so well documented in disease that its presence is considered a pathological hallmark of TDP-43 proteinopathy (6,8).

TDP-43 has four major domains: an oligomerizing, folded N-terminal region, two RNA recognition motifs, and an intrinsically disordered, C-terminal LCD (3,9).

Submitted April 28, 2023, and accepted for publication January 2, 2024.
*Correspondence: wks3@case.edu
Editor: Scott Showalter.
https://doi.org/10.1016/j.bpj.2024.01.001

The LCD (residues ~267–414), especially, has been a topic of immense interest as C-terminal fragments of TDP-43 containing the LCD are enriched in protein inclusions isolated from patients (1,2,10). The LCD is believed to drive TDP-43 amyloid aggregation (3,11–13), and the vast majority of disease-related mutations of TDP-43 map to this domain (3,14). Furthermore, recent reports point to the importance of the LCD to liquid-liquid phase separation (LLPS) of TDP-43 (15–17), a phenomenon whereby protein undergoes condensation, forming reversible, liquid-like droplets (18–20). An evolutionarily conserved segment of the LCD encompassing residues ~320–340 plays an especially important role in this regard (15,16,21). Indeed, deletion of this segment, which has a propensity to adopt α-helical structure (15,22,23) has been shown to cause severe inhibition and even abrogation of LLPS (16,24).

Although there has been an increasing appreciation for the physiologic role LLPS plays in spatially organizing cells (18,19,25), a rapidly growing body of evidence points to a darker side of this phenomenon, indicating that LLPS (or its dysregulation) of RNA-binding proteins such as TDP-43 may play an important role in the pathogenesis of neurodegenerative disorders by facilitating protein aggregation and disrupting downstream cellular processes (20,26–29). In this context, research of TDP-43 LLPS has exploded in recent years, leading to new insights into the driving forces and modulators of TDP-43 phase separation (5,21,24,30,31). This progress notwithstanding, however, little is known regarding the role of post-translational modifications (PTMs) in TDP-43 LLPS. This knowledge gap is especially striking with regard to phosphorylation, a PTM that is a hallmark of brain pathology (1,2,6,8,32–34). Furthermore, the few studies that have addressed this issue have focused mainly on C-terminal phosphorylation sites of the LCD (e.g., S403, S404, S409, and S410) (35) and, to a lesser degree, an N-terminal phosphorylation site (i.e., S48) (36), leaving other known TDP-43 phosphorylation sites largely unexplored.

In this report, we used a phosphomimetic approach to determine the impact of phosphorylation at residues S332 and S333 on TDP-43 LLPS LCD and aggregation. These phosphorylation sites, which map to the critical transiently α-helical region of the LCD, have both been detected in ALS (32). Our data reveal that the phosphomimetic S332D and S333D substitutions greatly suppress the protein's ability to undergo LLPS and indicate that this suppression is largely due to the reduction of α-helical propensity within residues ~320–340 of the phosphomimetic protein variant. Furthermore, our data indicate that phosphomimetic substitutions at Ser332 and Ser333 significantly slow TDP-43 LCD droplet aging and protein aggregation into amyloid fibrils, suggesting that TDP-43 phosphorylation is not necessarily pathological.

MATERIALS AND METHODS

Expression and purification of WT and S333D TDP-43

Site-directed mutagenesis was employed on a plasmid encoding the sequence for wild-type (WT) TDP-43 LCD (residues 267–414) with an N-terminal His_6 tag and thrombin cleavage site (MRGSHHHHHHLVPRGS) to generate an analogous plasmid construct for S333D TDP-43 LCD in a pRSET-B vector. The proteins were expressed in Rosetta *Escherichia coli* and purified as previously described (30), with the notable exception that the N-terminal tag was cleaved with thrombin protease (Cytiva Life Sciences, Marlborough, Massachusetts) after FPLC and before HPLC. Briefly, post-FPLC protein product was diluted 16-fold into a solution of 20 mM potassium phosphate (pH 6). Thrombin was immediately added at a ratio of 10 U thrombin:1 mg of uncleaved TDP-43 LCD, and the mixture was rocked for 48 h at room temperature. The flocculent cleaved product was then concentrated fourfold, and subsequently mixed with double the volume of 8 M guanidinium hydrochloride for 30 min until the solution clarified. The solution was then concentrated once more, run on HPLC, and lyophilized as we detailed in a prior study (30).

^{15}N-labeled TDP-43 LCD was made using a slightly altered protocol. Protein was expressed overnight in BL21 (DE3) *Escherichia coli* in minimal media (pH 7, 6 g/L Na_2HPO_4, 3 g/L KH_2PO_4, 0.5 g/L NaCl, 1 g/L $^{15}NH_4Cl$ (Cambridge Isotope Laboratories, Tewksbury, Massachusetts), 11.1 g/L $CaCl_2$, 120.4 g/L $MgSO_4$, 3 g/L glucose) supplemented with 200 μL of thiamine (5 mg/mL) and 200 μL of biotin (5 mg/mL) per liter of media. To make ^{15}N/^{13}C-labeled TDP-43 LCD for 3D nuclear magnetic resonance (NMR) experiments, the glucose in the media was ^{13}C-labeled (Cambridge Isotope Laboratories, Tewksbury, Massachusetts). After overnight expression, the same protocol described above was used to purify the NMR-active protein. Before experiments, the concentrations of protein stocks were determined by absorbance at 280 nm using an extinction coefficient of 17,990 M^{-1} cm^{-1}.

Turbidity measurements

Phase separation was measured by turbidity (absorbance at 600 nm) at 25°C using a Tecan (Baldwin Park, California) Spark multimode microplate reader with Te-Cool active temperature control. Experiments were conducted in 20 mM potassium phosphate buffer (pH 7.4).

Fluorescence microscopy imaging

TDP-43 LCD was prepared in 20 mM potassium phosphate buffer (pH 7.4) with a varying concentration of NaCl. Samples were visualized by fluorescence microscopy using Alexa Fluor 488- or Alexa Fluor 594-labeled protein probe, with a 1:20 ratio of labeled-to-unlabeled protein. 20 μL volumes of sample were deposited on the bottom of 35-mm dishes precoated with 1% Pluronic F-127 (Sigma Aldrich, St. Louis, Missouri), and then images were collected at room temperature on a Keyence (Itasca, Illinois) BZ-X710 microscope with a ×100/1.45 numerical aperture oil-immersion lens.

To make the fluorescent probe, TDP-43 LCD was labeled with the appropriate Alexa Fluor NHS (succinimidyl) ester by adding 10 μL of dye in DMSO (10 mg/mL) to 100 μL of the protein (10 mg/mL) in 20 mM potassium phosphate (pH 7) buffer with 4 M guanidinium hydrochloride. The labeling reaction was conducted at room temperature for 1 h, under constant vortex mixing, and excess dye was cleared by using Zeba desalting columns (Thermo Fisher Scientific, Waltham, Massachusetts).

For recruitment studies, a mixture of WT TDP-43 LCD and S333D TDP-43 LCD was prepared in 20 mM potassium phosphate buffer (pH 7.4) containing 150 mM NaCl, with the final concentration of one of the proteins being above its saturation concentration and the final concentration of the other protein being below its saturation concentration. The former was

added first to the mixture, leading to initial droplet formation, followed by the latter. The mixture was then imaged as described above.

For miscibility studies, both proteins were prepared separately in 20 mM potassium phosphate buffer (pH 7.4) containing 150 mM NaCl, at 2× the final intended protein concentration of each variant. The final intended protein concentrations for both WT TDP-43 LCD and S333D TDP-43 LCD were above the proteins' respective saturation concentrations. The separate, droplet-containing protein preparations were then mixed and then imaged as described above.

NMR spectroscopy

The NMR experiments were carried out using a Bruker Scientific Instruments (Billerica, Massachusetts) Avance 900 MHz spectrometer equipped with an HCN TXI-Cryogenic Probe, maintained at a temperature of 25°C. Samples of unmodified WT TDP-43 LCD and phosphomimetic S333D TDP-43 LCD, isotopically labeled with either ^{15}N or both ^{13}C and ^{15}N, were prepared at a concentration of 60 μM and 20 μM protein in MES buffer (pH 6.1). Each experiment was run on different sample preparations. The raw NMR data were processed using NmrPipe software and further reconstructed using Smile software (37,38). Finally, the processed data were analyzed using NMRFAM Sparky software (39).

Backbone amide resonance assignments were determined by performing ^{1}H-^{15}N HSQC and standard Bruker three-dimensional triple-resonance experiments, including HNCA (40–44), HN(co)CA (40,42,44), and CBCAcoNH (45,46) with nonuniform sampling. From these data, Cα and Cβ secondary chemical shifts ($\Delta\delta C_\alpha$ and $\Delta\delta C_\beta$, respectively) were calculated at 20 μM and at 60 μM protein for each detectable residue in both TDP-43 LCD variants by subtracting the chemical shift of that residue in a random coil from the observed chemical shift ($\Delta\delta = \delta_{observed} - \delta_{random\ coil}$) (15,47,48). Random coil chemical shift values were obtained from the Poulsen IDP/IUP random coil shifts calculator (default parameters and the experimental temperature were inputted) (49,50). $\Delta\delta C_\alpha$-$\Delta\delta C_\beta$ was then determined for every detectable as a readout of local secondary structure (15,48).

FRAP

Droplets of WT TDP-43 LCD (25 μM) and S333D TDP-43 LCD (55 μM) were prepared in 20 mM potassium phosphate buffer (pH 7.4) containing 150 mM NaCl. Alexa Fluor 488-labeled protein (prepared as described in the section, fluorescence microscopy imaging) was added such that the ratio of labeled-to-unlabeled protein was 1:140. Droplets were allowed to age to the desired timepoint in a 1.5 mL Eppendorf tube and then deposited on the bottom of a 35-mm dish precoated with 1% Pluronic F-127 (Sigma Aldrich, St. Louis, Missouri) before being covered with a glass coverslip. Fluorescence recovery after photobleaching (FRAP) measurements were taken with a Leica Microsystems (Deerfield, Illinois) HyVolution SP8 confocal microscope using 2.4-mW laser intensity for bleaching, ×63/1.4 numerical aperture oil-immersion objective, and a photo-multiplier tube detector. Due to the small sizes of the droplets (~1 μm in diameter), the entire droplet was photobleached. Four prebleaching frames, six flashes of bleaching (62% of laser power), and 100 postbleaching frames (1.3 s/frame) were collected. Each FRAP trace was normalized to maximal prebleach and minimal postbleach intensities.

Thioflavin T fluorescence assay

All fibrillation reactions were conducted at 25°C in 20 mM potassium phosphate buffer (pH 7.4) containing 150 mM NaCl and 15 μM ThT. ThT fluorescence was measured on a Tecan (Baldwin Park, California) Spark plate reader at 20-min intervals, with 5 s of linear agitation (amplitude 1 mm) before each reading (excitation and emission wavelengths of 440 and 485 nm, respectively). Half-times of the reactions were ascertained by normalizing the resultant traces to the maximal ThT fluorescence intensity of the plateau phase and determining when 50% of that maximal signal was reached.

Atomic force microscopy imaging

Atomic force microscopy was done as previously described (30). Fibrils collected during the plateau phase of fibrillation reactions were deposited on freshly cleaved mica discs, left at ambient temperature for 5 min, and then washed five times with Milli-Q H_2O before being dried under N_2 gas. Images were collected in scan assist mode using a silicon probe (spring constant: 40 N/m) on a Bruker Scientific Instruments (Billerica, Massachusetts) multimode atomic force microscope with a Nanoscope V controller. Nanoscope Analysis software was utilized for image processing.

RESULTS

S332D and S333D phosphomimetic substitutions inhibit liquid-liquid phase separation of TDP-43 LCD

It has been previously established that the transiently α-helical region (residues ~320–340) of TDP-43's low-complexity domain (LCD) is critical to the protein's ability to engage in protein-protein interactions, including those that mediate LLPS (15,16,21,23,24,30,47). Indeed, pathological mutations within this region have been shown to significantly impact the formation of droplets and their properties (3,15,47). Studies done both in vitro and with patient tissue have detected phosphorylation sites, Ser332 and Ser333, within this transiently α-helical region (32,51). Thus, we asked whether phosphorylation at these residues affects the LLPS of the TDP-43 LCD.

To mimic phosphorylation, we introduced a phosphomimetic Ser-to-Asp substitution at the residue of interest to create S332D TDP-43 LCD or S333D TDP-43 LCD. This strategy is commonly employed to model phosphorylation, as it is easy to implement and results in a homogeneous population of precisely modified protein. We first investigated the effect of these substitutions on TDP-43 LCD LLPS by measuring turbidity (the optical density at 600 nm) at pH 7.4 as a function of NaCl concentration and by verifying the presence of droplets via fluorescence microscopy. WT TDP-43 LCD at 20 μM concentration underwent LLPS under these experimental conditions, with the extent of this reaction increasing strongly with increasing salt concentration, in accordance with other studies (15,23,30,47). In contrast, S332D TDP-43 LCD and S333D TDP-43 LCD at the same concentration did not undergo LLPS at all (Fig. 1 *A* and *B*).

To ascertain if these phosphomimetic substitutions completely abrogate TDP-43 LCD LLPS or merely suppress it, phase diagrams were constructed for all of the proteins by assessing LLPS as a function of protein and salt concentrations. These phase diagrams showed that S332D TDP-43 LCD and S333D TDP-43 LCD can phase separate, but that they do so at much higher protein concentrations than WT TDP-43 LCD under the same conditions (Fig. 1 *C*). Determining the saturation concentrations (c_{sat}), a widely used

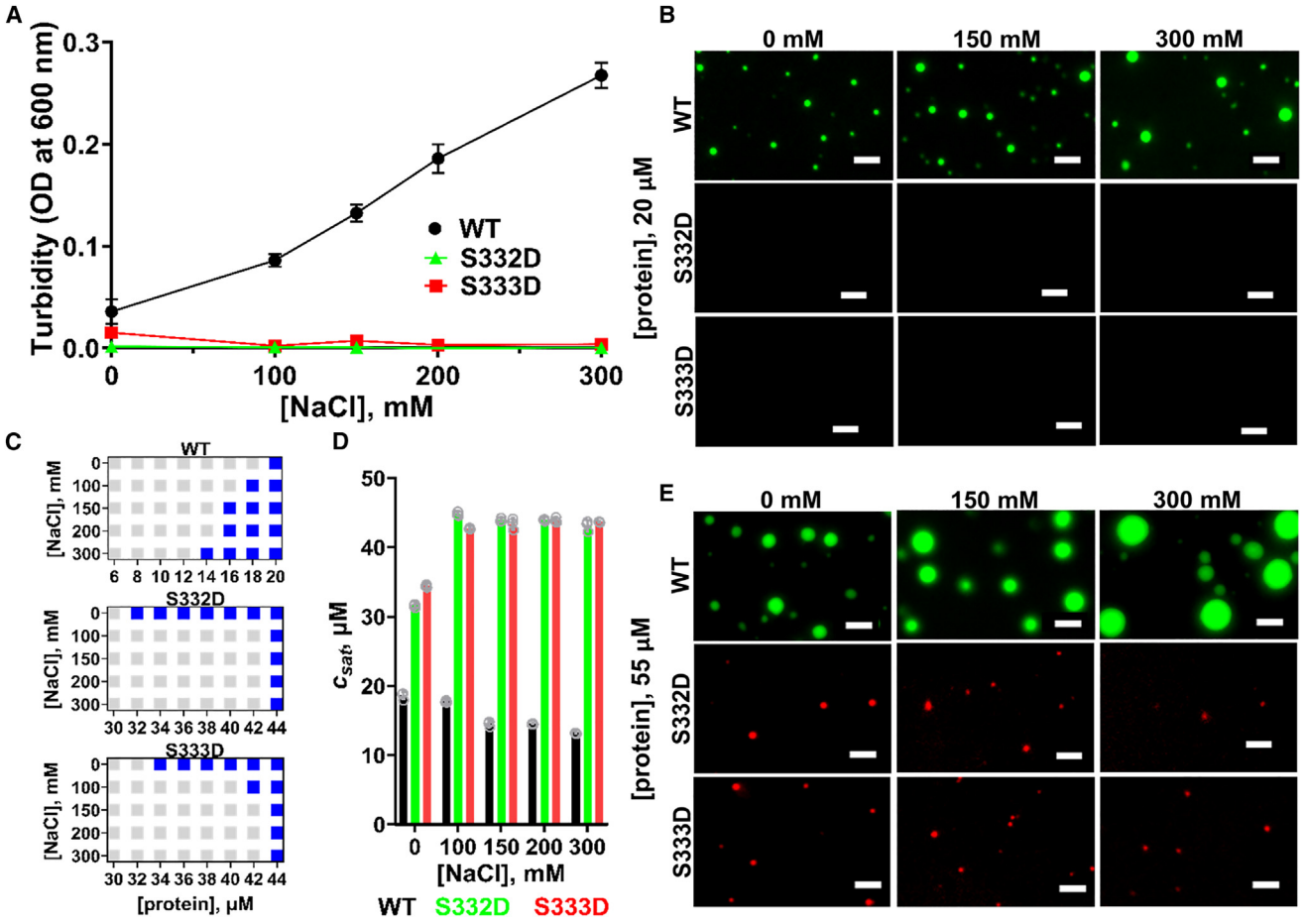

FIGURE 1 Phosphomimetic substitution within the transiently α-helical region inhibits TDP-43 LCD LLPS. (*A*) Turbidity of WT TDP-43 LCD, S332D TDP-43 LCD, and S333D TDP-43 LCD (20 μM in each case) as a function of NaCl concentration. Error bars represent SD (n = 3). (*B*) Representative fluorescence microscopy images of WT TDP-43 LCD (*top*), S332D TDP-43 LCD (*middle*), and S333D TDP-43 LCD (*bottom*) at 20 μM protein. (*C*) Protein concentration versus NaCl concentration phase diagrams for WT TDP-43 LCD (*top*), S332D TDP-43 LCD (*middle*), and S333D TDP-43 LCD (*bottom*). (*D*) Saturation concentrations of WT TDP-43 LCD, S332D TDP-43 LCD, and S333D TDP-43 LCD at different NaCl concentrations. Gray circles represent individual data points (n = 3). (*E*) Representative fluorescence microscopy images of WT TDP-43 LCD (*top*), S332D TDP-43 LCD (*middle*), and S333D TDP-43 LCD (*bottom*) at 55 μM protein. Proteins were labeled with Alexa Fluor 488 (WT TDP-43 LCD) or Alexa Fluor 594 (S332D and S333D TDP-43 LCD), and the ratio of labeled-to-unlabeled protein was 1:20 for each protein. Scale bar, 3 μm. Experiments were performed in 20 mM potassium phosphate buffer (pH 7.4). OD = optical density.

quantitative measure of a protein's propensity to undergo LLPS, underscored this point, as the c_{sat}'s of the phosphomimetic TDP-43 LCD variants were similar to each other but substantially higher than that of WT TDP-43 LCD under all conditions tested (Figs. 1 *D* and S1). Altogether, these data clearly demonstrate that TDP-43 LCD LLPS is inhibited by phosphomimetic substitution at Ser332 and Ser333. Furthermore, when formed, droplets of S332D TDP-43 LCD and S333D TDP-43 LCD were much smaller than those generated from the WT protein (Fig. 1 *E*).

S333D substitution results in disruption of the transiently α-helical region of TDP-43 LCD

We first hypothesized that the suppressive effect of S332D and S333D phosphomimetic substitutions on TDP-43 LCD LLPS was caused by the long-range repulsive intermolecular electrostatic interactions between the introduced negatively charged residues. However, increasing NaCl concentration did not restore LLPS of either TDP-43 LCD phosphomimetic variant (Fig. 1). In fact, in contrast to the behavior of the WT protein, higher salt concentrations appeared to diminish S332D and S333D TDP-43 LCD LLPS (Figs. 1 *C* and *D* and S1). Thus, this explanation was unlikely. Given this finding, next we tested whether the inhibitory effect on LLPS could be due to diminished α-helical propensity of the transiently α-helical region. Following the methodology established in the studies of Conicella et al. (15,47), dispersed-phase solution NMR spectroscopy was used on the S333D TDP-43 LCD variant to test this possibility.

First, the ^{1}H-^{15}N HSQC spectra of WT TDP-43 LCD and S333D TDP-43 LCD were collected at 20 μM protein, in pH

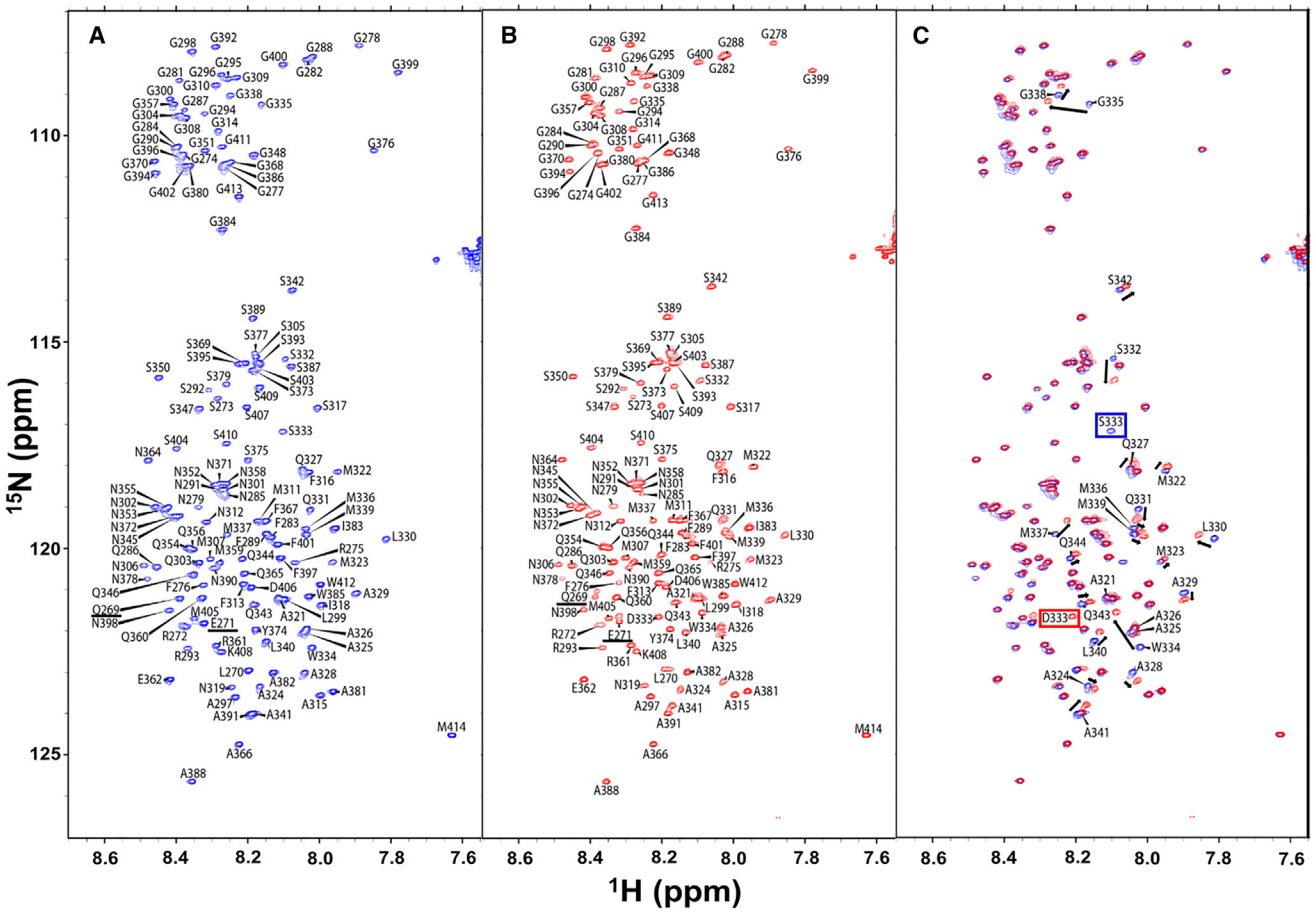

FIGURE 2 ^{1}H-^{15}N HSQC spectra of WT TDP-43 LCD and S333D TDP-43 LCD. (*A*) WT TDP-43 LCD. (*B*) S333D TDP-43 LCD. (*C*) Overlay of spectra for both proteins. Boxes indicate the mutated residue at position 333. Arrows indicate residues with chemical shift differences between the two proteins. Residues with differently shaped peaks between the two proteins are underlined. Experiments were performed in 20 mM MES buffer (pH 6.1) in the absence of salt.

6.1 MES buffer without salt, conditions that have been utilized successfully by other groups to study TDP-43 LCD via NMR (15,47). It should be noted that under these conditions, the saturation concentration of TDP-43 LCD is greater than 60 μM at room temperature, allowing for dispersed-phase NMR experiments at much higher protein concentrations than would be possible in phosphate buffer (Fig. S2). Both spectra showed a narrow range of chemical shifts in the ^{1}H dimension ($\sim$1 ppm), a hallmark of intrinsically disordered proteins (Fig. 2 *A* and *B*) (52). After obtaining complete chemical shift assignments, it was evident that the majority of the residues of S333D TDP-43 LCD matched exactly with those of WT TDP-43 LCD, with the exception of the substituted residues at position 333 and the rest of the residues within the transiently α-helical region (Fig. 2 *C*). Furthermore, residues 269 and 271 appeared as doublet peaks in the S333D HSQC. The reason for the apparent doublet peaks of these residues in the S333D HSQC is unclear (it is possible these could be due to deamidation of the residues in a small fraction of the S333D protein), but it ultimately does not affect the interpretation of our results given these residues are not near the transiently α-helical region. The differences between the proteins in the chemical shifts of the transiently α-helical region residues suggested differences in the secondary structure within this region between WT TDP-43 LCD and S333D TDP-43 LCD.

To characterize these structural differences between WT TDP-43 LCD and S333D TDP-43 LCD in greater detail, we determined ^{13}C secondary chemical shift values for the α-carbon ($\Delta\delta C_\alpha$) and β-carbon ($\Delta\delta C_\beta$) of each detectable residue of both proteins (Table S1). Secondary chemical shift values report on local secondary structure, and computing $\Delta\delta C_\alpha$-$\Delta\delta C_\beta$ for each residue in a protein is a highly sensitive approach to determining α-helical structure, with stretches of consecutive positive $\Delta\delta C_\alpha$-$\Delta\delta C_\beta$ values $>$ 0.8 ppm indicating significant α-helical content (15,53). Residue 333 was excluded from this analysis for both proteins. For WT TDP-43 LCD at 20 μM protein, significant α-helical secondary structure was found for residues 320–331; additionally, minor α-helical secondary structure was found for residues 332–343, as indicated by consecutive

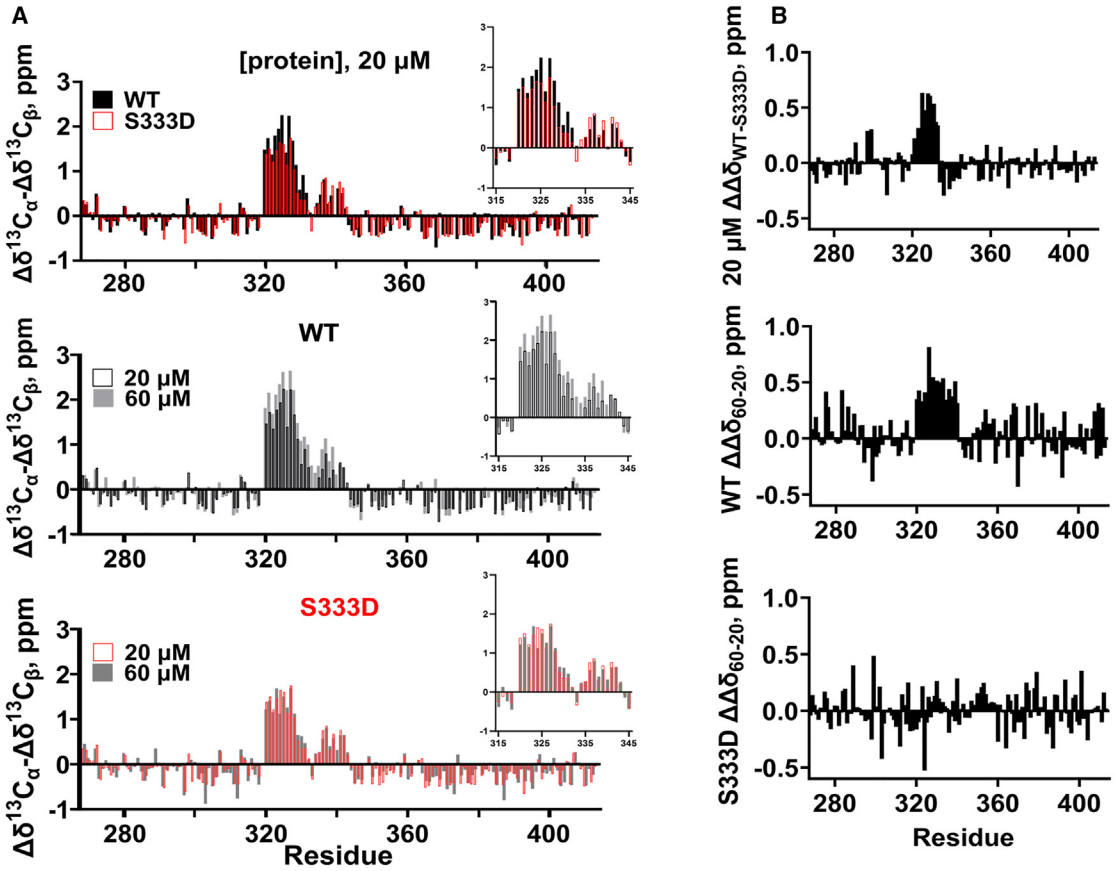

FIGURE 3 ^{13}C secondary chemical shift ($\Delta\delta C_\alpha$-$\Delta\delta C_\beta$) profiles of WT TDP-43 LCD and S333D TDP-43 LCD. (*A*) Secondary chemical shifts of WT TDP-43 LCD and S333D TDP-43 LCD at 20 μM (*top*), WT TDP-43 LCD at 20 and 60 μM (*middle*), and S333D TDP-43 LCD at 20 and 60 μM (*bottom*). Inserts show data for residues 315–345, encompassing the entire transiently α-helical region. (*B*) Differences in secondary chemical shifts ($\Delta\Delta\delta$) between WT and S333D TDP-43 LCD at 20 μM (*top*), WT TDP-43 LCD at 20 and 60 μM (*middle*), and S333D TDP-43 LCD at 20 and 60 μM (*bottom*). Experiments were performed in 20 mM MES buffer (pH 6.1) in the absence of salt.

positive $\Delta\delta C_\alpha$-$\Delta\delta C_\beta$ values < 0.8 ppm along this 12-residue stretch (Fig. 3 *A*, *top*). This is fully consistent with the previously published data for the WT protein (15, 47, 48). For S333D TDP-43 LCD at the same concentration, however, significant α-helical secondary structure was found for residues 320–328 only and minor α-helical secondary structure for residues 329–343 (Fig. 3, *top*). These results suggested that the transiently α-helical region of S333D TDP-43 is shorter than that of WT TDP-43. Furthermore, the $\Delta\delta C_\alpha$-$\Delta\delta C_\beta$ values for residues 320–332 of WT TDP-43 LCD are greater than those of S333D TDP-43 LCD (Fig. 3 *B*, *top*), signifying a lower α-helical tendency along this stretch in the phosphomimetic protein.

Intermolecular helix-helix protein contacts are known to stabilize and extend the transiently α-helical region of WT TDP-43 LCD (15,23,47). To determine if S333D phosphomimetic substitution alters this behavior, we performed dispersed-phase NMR experiments on both proteins at 60 μM (Fig. S3; Table S1). At this higher protein concentration, TDP-43 LCD multimerization is promoted, and the NMR signal becomes a weighted average of multimeric TDP-43 complexes (which broaden the signal due to their faster T_2 relaxation rates) and the remaining monomers in the presence of said complexes (15,23,47,52). NMR spectroscopy at higher protein concentrations can thus be used to probe conformational changes that TDP-43 LCD undergoes as a result of multimerization (15,52). For WT TDP-43 LCD, increasing protein concentration from 20 to 60 μM increased $\Delta\delta C_\alpha$-$\Delta\delta C_\beta$ values, indicating an enhanced α-helical tendency for residues 320–340 (Fig. 3 *A*, *middle*, and *B*, *middle*), again in full agreement with the previous reports in the literature (15,47). In contrast, for S333D TDP-43 LCD, there was no measurable difference between $\Delta\delta C_\alpha$-$\Delta\delta C_\beta$ profiles as protein concentration was increased from 20 to 60 μM (Fig. 3 *A*, *bottom*, and *B*, *bottom*), indicating a lack of difference in secondary structural propensity. Thus, it appeared that the S333D phosphomimetic substitution not only disrupts the transiently α-helical region, but it also inhibits the region from stabilizing its secondary structure via intermolecular protein-protein interactions at higher protein concentrations (Figs. 3 and S3). To further test this hypothesis, we introduced a helix-enhancing S333A mutation to the TDP-43 LCD and found that the saturation concentrations for this mutant were much lower than those of WT

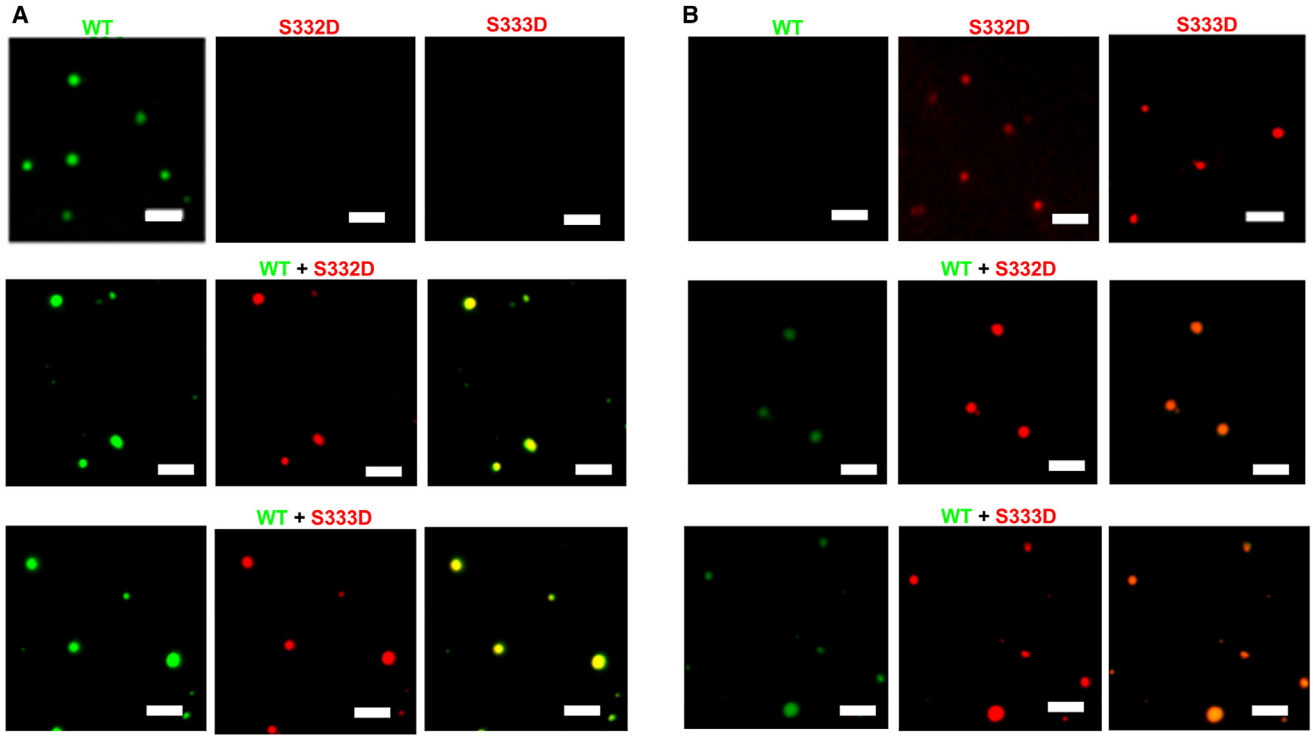

FIGURE 4 WT TDP-43 LCD and phosphomimetic TDP-43 LCD variants exhibit reciprocal recruitment. (*A*) Representative fluorescence microscopy images of WT TDP-43 LCD (25 μM, i.e., above c_{sat}), S332D TDP-43 LCD (5 μM, i.e., below c_{sat}), and S333D TDP-43 LCD (5 μM, i.e., below c_{sat}). Images in top panels were obtained for individual proteins separately, and the images in the middle and bottom panels were obtained for the mixture of WT protein with a phosphomimetic variant. (*B*) Representative fluorescence microscopy images of WT TDP-43 LCD (5 μM, i.e., below c_{sat}), S332D TDP-43 LCD (55 μM, i.e., above c_{sat}), and S333D TDP-43 LCD (55 μM, i.e., above c_{sat}). Images in top panels were obtained for individual proteins separately, and the images in the middle and bottom panels were obtained for the mixture of WT protein with a phosphomimetic variant. Proteins were labeled with Alexa Fluor 488 (WT TDP-43 LCD) or Alexa Fluor 594 (S332D and S333D TDP-43 LCD), and the ratio of labeled-to-unlabeled protein was 1:20 for each protein. Scale bar, 3 μm. Experiments were performed in 20 mM potassium phosphate buffer (pH 7.4) containing 150 mM NaCl.

protein under the same conditions (Fig. S4). This finding offers a mechanistic explanation as to why LLPS of TDP-43 LCD is suppressed upon phosphomimetic substitution within the transiently α-helical region.

S332D TDP-43 LCD and S333D TDP-43 LCD remain recruitable by and miscible with WT TDP-43 LCD droplets

Protein droplets formed through LLPS can recruit biomolecules such as nucleic acids or other proteins from the surrounding bulk solution, concentrating such species within them (54–56). PTMs have been shown to modulate this process in other protein systems (57), prompting us to investigate whether phosphomimetic TDP-43 LCD can be recruited to WT TDP-43 LCD droplets. To this end, WT TDP-43 LCD was mixed with either S332D TDP-43 LCD or S333D TDP-43 LCD under physiologically relevant buffer conditions (pH 7.4, 150 mM NaCl) at concentrations where the WT protein alone phase separates, but S332 TDP-43 LCD and S333D TDP-43 LCD do not (Fig. 4 *A*, *top*). Microscopy revealed that the phosphomimetic proteins were present with WT TDP-43 LCD in every droplet examined (Fig. 4 *A*, *middle* and *bottom*), suggesting robust recruitment of the phosphomimetic protein to droplets formed by WT TDP-43 LCD. The converse experiment, in which the proteins were mixed at concentrations where S332D TDP-43 LCD and S333D TPD-43 LCD on their own form droplets but WT TDP-43 LCD does not (Fig. 4 *B*, *top*), yielded similar results. WT TDP-43 LCD was present in all droplets along with the phosphomimetic variant, (Fig. 4 *B*, *middle* and *bottom*), showing reciprocal recruitment of each protein to droplets formed by the other protein.

We next asked how the proteins behave under conditions in which both can homotypically phase separate. WT TDP-43 LCD and S332D TDP-43 LCD or WT TDP-43 LCD and S333D TDP-43 LCD were mixed together under appropriate conditions (i.e., at concentrations above c_{sat} values of both proteins), at physiologically relevant pH and salt concentration, and the samples were examined under a microscope (Fig. 5 *A*). The droplets formed in this experiment again contained WT TDP-43 and phosphomimetic TDP-43, and the proteins in each preparation were homogenously distributed (Fig. 5 *B* and *C*). This finding indicated that not only does WT protein co-localize to the same droplets as the phosphomimetic proteins, but that WT TDP-43 and

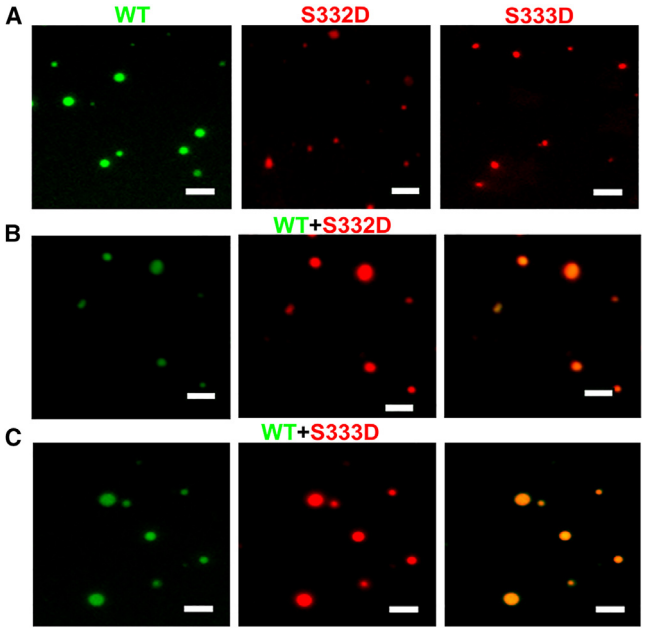

FIGURE 5 WT TDP-43 LCD and phosphomimetic TDP-43 LCD variants are miscible within droplets. (*A*) Representative fluorescence microscopy images of WT TDP-43 LCD (25 μM), S332D TDP-43 LCD (55 μM), and S333D TDP-43 LCD (55 μM) separately. (*B* and *C*) Representative fluorescence microscopy images for the mixture of (*B*) 25 μM WT TDP-43 LCD and 55 μM S332D TDP-43 LCD and (*C*) 25 μM WT TDP-43 LCD and 55 μM S333D TDP-43 LCD. Green channel (*left*), red channel (*middle*), and merged (*right*) images are shown. Proteins were labeled with Alexa Fluor 488 (WT TDP-43 LCD) or Alexa Fluor 594 (S332D and S333D TDP-43 LCD), and the ratio of labeled-to-unlabeled protein was 1:20 for each protein. Scale bar, 3 μm. Experiments were performed in 20 mM potassium phosphate buffer (pH 7.4) containing 150 mM NaCl.

the phosphomimetic TDP-43 are miscible within these droplets. Thus, phosphomimetic substitution at residue 332 or 333 of the TDP-43 LCD does not affect its recruitment to or miscibility with WT protein.

Phosphomimetic substitutions within the transiently α-helical region inhibit TDP-43 LCD droplet aging

Phase-separated condensates are usually highly dynamic and reversible when newly formed. However, for some proteins, there is a transition with time from a liquid-like state to a more rigid state. This process, referred to as droplet aging, often has pathological consequences (27,29,30). Droplet aging can be studied by monitoring the physiochemical properties (e.g., density, viscosity, surface tension) of the condensates or the macromolecular diffusion between droplets and the bulk phase over time. FRAP is a technique to measure the latter, and it is what we employed to compare WT TDP-43 LCD and phosphomimetic TDP-43 LCD droplet aging.

Because droplets of S332D TDP-43 LCD and S333D TDP-43 LCD are small (~1 micron in diameter), it was impractical to photobleach the center of the droplets only. Instead, in our experiments, we photobleached the entire condensate (Fig. 6 *B*). Even though freshly prepared WT TDP-43 LCD droplets were dynamic, they underwent relatively fast aging, exhibiting only ~65% recovery of fluorescence as early as 20 min after preparation (the earliest time point we could measure in our experiments). The extent of this recovery diminished further with time, falling to 23% after 4 h of incubation (Fig. 6 *A*, *left*). By contrast, S332D and S333D protein droplets aged substantially more slowly, showing ~70% recovery of fluorescence signal even after 4 h of incubation. It took as long as 24 h for these droplets to show significant aging (Fig. 6 *A*, *middle* and *right*). Overall, these data clearly indicate that the phosphomimetic S332D and S333D substitutions profoundly slow the aging of TDP-43 LCD droplets.

Phosphomimetic substitutions within the transiently α-helical region slow down TDP-43 LCD fibrillation

A hallmark for many neurodegenerative diseases is the accumulation of amyloid fibrils in the central nervous system. For some LLPS-prone proteins, droplet rigidification has been shown to precede formation of such fibrillar aggregates (27–29,58). Therefore, next we tested the impact of the S332D and S333D phosphomimetic substitutions on TDP-43 LCD fibrillation. Although ideally one would want to follow the fibrillation reaction exclusively within the condensed phase, this proved to be impractical for our system due to relatively high concentrations of proteins (as indicated by the c_{sat} values of WT TDP-43 LCD, S332D TDP-43 LCD, and S333D TDP-43 LCD (Figs. 1 *D* and S1)), and thus considerable fibrillation rates, in the dilute phase outside the droplets. Therefore, we performed these experiments under conditions where none of the proteins was able to undergo LLPS (10 μM protein, 20 mM pH 7.4 potassium phosphate buffer with 150 mM NaCl), using the standard Thioflavin T (ThT) fluorescence assay. This approach avoided having to discriminate fibrillation occurring inside the bulk phase from fibrillation occurring in the condensates, allowing unambiguous interpretation of our results. As shown in Fig. 7 *A*, the fibrillation rates under these conditions of S332D TDP-43 LCD and S333D TDP-43 LCD were substantially reduced compared with that of the WT protein, with reaction half-times of 22.3 $\pm$ 1.4, 17.0 $\pm$ 1.3, and 10.1 $\pm$ 1.7 h, respectively. The slower fibrillation rates of phosphomimetic TDP-43 LCD correlate well with the reduced rates at which these variants undergo rigidification within the environment of the condensed phase (Fig. 6 *A*). It should also be noticed that the maximum ThT signals of the S332D and S333D variants were significantly lower than that of the WT protein. This likely reflects lower binding affinity of the negatively charged ThT to fibrils formed from the phosphomimetic variants and/or

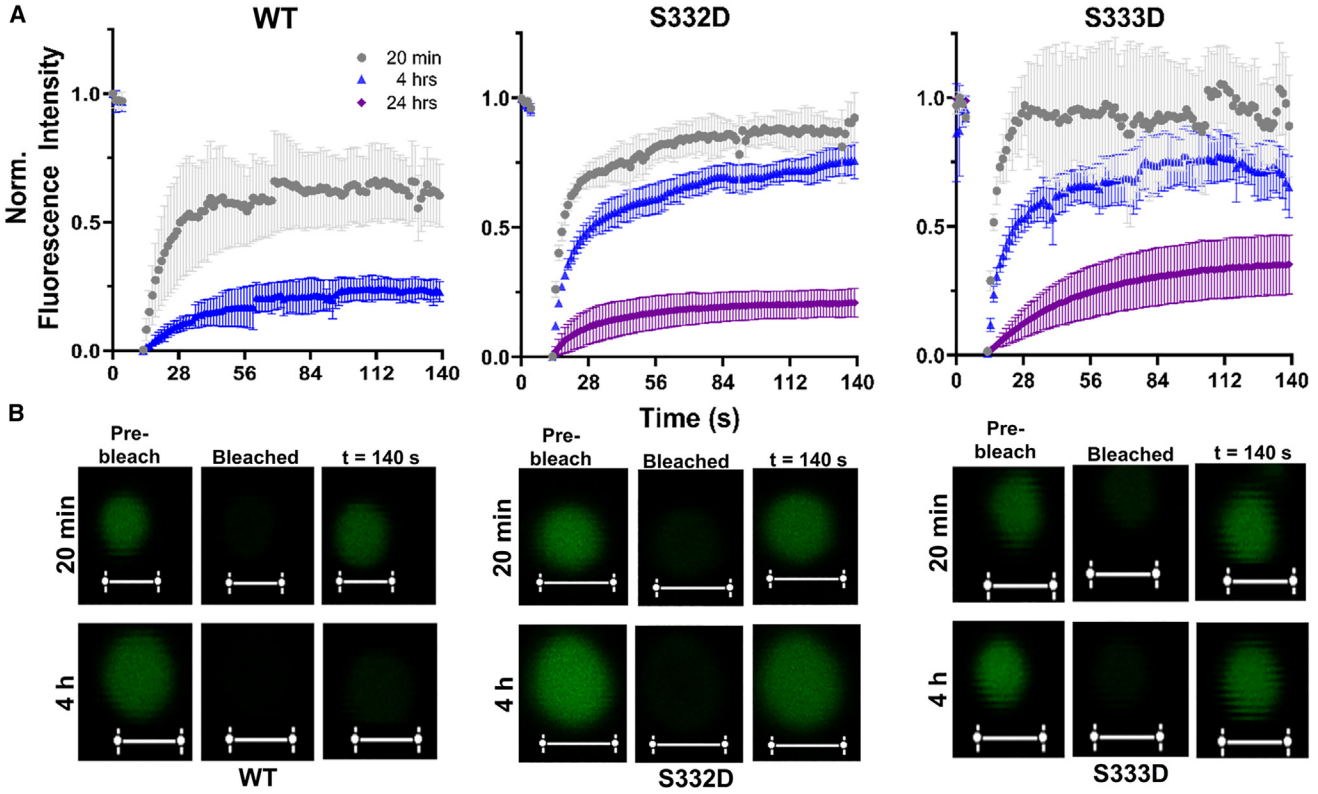

FIGURE 6 Phosphomimetic mutation within the transiently α-helical region slows TDP-43 LCD droplet aging. (*A*) Representative FRAP traces for WT TDP-43 LCD droplets (prepared at 25 μM protein, *left*), S332D TDP-43 LCD droplets (prepared at 55 μM protein, *middle*), and S333D TDP-43 LCD droplets (prepared at 55 μM protein, *right*). The data were obtained 20 min, 4 h, or 24 h after LLPS induction. Error bars represent SD ($n \geq 5$). (*B*) Representative confocal images of WT TDP-43 LCD droplets (*left*), S332D TDP-43 LCD droplets (*middle*), and S333D TDP-43 LCD droplets (*right*) during FRAP experiments. Images in the top row depict droplets 20 min after induction of LLPS, and those in the bottom row depict droplets 4 h after induction of LLPS. Proteins were labeled with Alexa Fluor 488, and the ratio of labeled-to-unlabeled protein was 1:140 for each protein. Scale bar, 1 μm. Experiments were performed in 20 mM potassium phosphate buffer (pH 7.4) containing 150 mM NaCl.

potential structural differences between the fibrils, even though they appear very similar at the gross morphological level (Fig. 7 *B*).

DISCUSSION

The observation that many proteins within the aggregates that characterize age-related neurodegenerative diseases have high propensities to form condensates through the mechanism of LLPS has spurred studies of LLPS as a potentially pathogenic process (20,27–29,59). The LLPS of TDP-43, especially, has received intense attention as this nucleocytoplasmic protein is associated with several severely debilitating neurodegenerative disorders, including amyotrophic lateral sclerosis, frontotemporal dementia, limbic age-related TDP encephalopathy, and Alzheimer's disease (1–5). Such studies have revealed that the C-terminal LCD of TDP-43, which was already of great interest due to the enrichment of TDP-43 C-terminal fragments in proteinaceous inclusions in disease (1, 2, 10), is the primary driver of its LLPS (15,23,30,47). Furthermore, these investigations have yielded valuable insights into the forces underpinning TDP-43 LLPS and the link between TDP-43 LLPS and aggregation (3,5,16,21,27,31). A critical gap, however, exists in our current understanding of the role of PTMs in TDP-43 phase separation. In particular, TDP-43 phosphorylation is widespread in disease, to the point that the presence of phosphorylated TDP-43 is used as a biomarker of TDP-43 proteinopathy (6,8). However, little is known about the impact of this type of post-translational modification on the protein's phase separation. The few studies that have addressed this issue have focused on phosphorylation sites within the N-terminal TDP-43 domain (36) and at the very C-terminal end of the LCD (35), largely ignoring those that have been identified in other regions of the protein (34). In an effort to bridge this knowledge gap, this study examined the effects of phosphorylation at residues S332 and S333 on the LLPS and fibrillation of the TDP-43 LCD using a phosphomimetic model. Phosphorylation at these sites, which have been identified in diseased brain tissue (32), is of singular interest as it lies within the transiently α-helical region, a critical subdomain of the protein.

Many groups have reported that LLPS of the WT TDP-43 LCD is promoted by increasing salt concentration, a behavior that is attributed to screening out the repulsive,

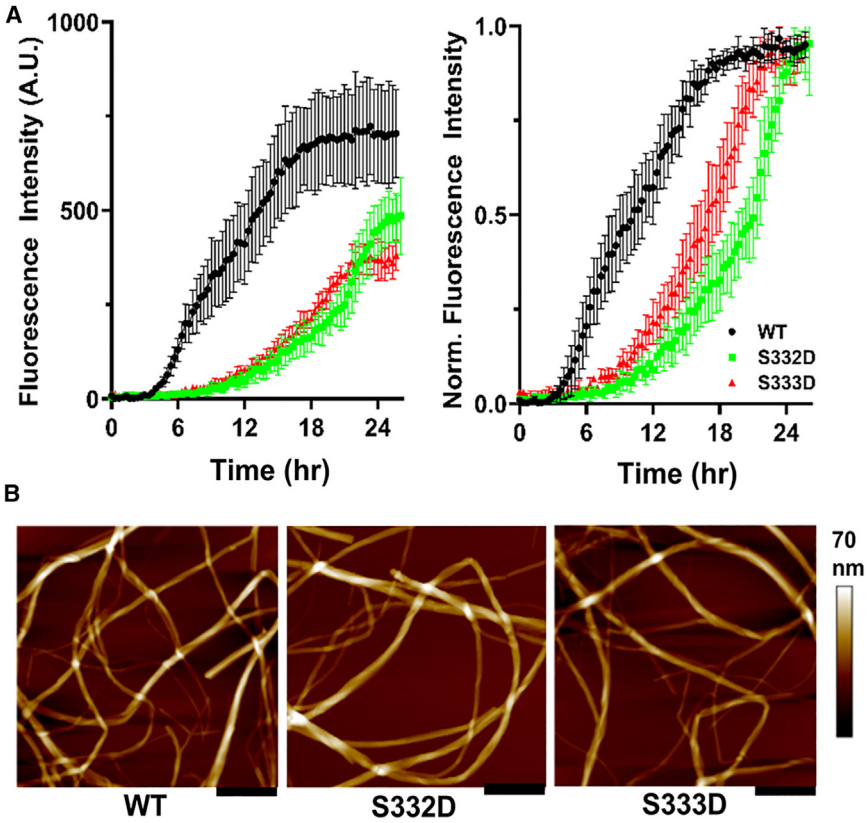

FIGURE 7 S333D and S332D phosphomimetic mutation slows TDP-43 LCD aggregation. (*A*) ThT fluorescence traces of WT TDP-43 LCD, S332D TDP-43 LCD, and S333D TDP-43 LCD (10 μM, i.e., below c_{sat} for each protein). The traces on the left show raw values, and the traces on the right show values normalized to the maximum signal during the plateau phase. A.U. = arbitrary units. Error bars represent SD (n = 3–7). (*B*) Representative atomic force microscopy images of WT TDP-43 LCD (*left*), S332D TDP-43 LCD (*middle*), and S333D TDP-43 LCD (*right*). Fibrils were collected at 25 h of incubation (i.e., after the proteins had entered the plateau phase). Scale bar represents 400 nm. Experiments were conducted in 20 mM pH 7.4 buffer containing 150 mM NaCl.

long-range intermolecular electrostatic interactions and/or increasing the attractive hydrophobic interactions that govern the WT protein's phase separation (15,23,30,47). Our study recapitulated these findings, confirming that the unmodified WT protein at 20 μM concentration undergoes LLPS at physiologic pH and salt concentrations, and that this condensation becomes even more robust at higher salt concentrations. In sharp contrast, phosphomimetic S332D TDP-43 LCD and S333D TDP-43 LCD showed no LLPS under similar conditions, and phase separation of these phosphomimetic variants could only be observed at substantially higher protein concentration. Overall, this indicated that phosphomimetic substitutions at residues S332 and S333 greatly inhibited TDP-43 phase separation. Furthermore, droplets formed by S332D TDP-43 LCD and S333D TDP-43 LCD were much smaller compared with those formed by the unmodified TDP-43 LCD, although droplet size per se is not a measure of LLPS propensity. The transiently α-helical region of the TDP-43 LCD, a segment spanning residues ~320–340, is known to be essential for intermolecular protein-protein interactions, including those that underlie homotypic LLPS (15,16,21,23,24,47). In fact, it was shown that TDP-43 LCD LLPS is abrogated when this region is deleted or its secondary structure is interrupted (16,24). As our phosphomimetically modified residues introduced a negative charge to this natively uncharged and hydrophobic subdomain, we initially suspected a repulsive electrostatic mechanism to be at least partly responsible for the observed inhibition of LLPS. The finding that increasing salt concentration failed to restore LLPS of the phosphomimetic variant argued against this possibility; higher salt concentrations actually further inhibited its phase separation, the opposite of what is observed with WT protein. This could potentially be a result of salt interfering with attractive intermolecular electrostatic interactions between the positively and negatively charged residues of TDP-43, which may be more significant in the context of the phosphomimetic proteins given their additional negative charge (35) and (as discussed later) their suppressed transient α-helical structure. This is, however, an admittedly somewhat speculative explanation. Furthermore, it should be mentioned that a recent study with an ALS-associated G335D TDP-43 LCD mutant reported that this mutation resulted in an increased LLPS propensity (47), further arguing against the possibility that repulsive electrostatic interactions could fully explain the reduced LLPS propensity of the phosphomimetic proteins used in our present study.

Structural investigations of the transiently α-helical region via dispersed-phase solution NMR yielded insight into the actual mechanism at work. These experiments showed that the S333D phosphomimetic substitution disrupted, but did not completely abolish, the helical secondary structure of this region. Furthermore, our data revealed that the

stabilization and extension of the transiently α-helical region that occur upon increasing WT TDP-43 LCD concentration (15) were not observed for S333D TDP-43 LCD. Thus, the suppression of TDP-43 LCD LLPS by the S333D substitution appears to be, at least in part, due to the disruption of its transiently α-helical region, as such an effect would disrupt the intermolecular contacts this region mediates that are vital to TDP-43 LLPS (15,16,21,23,47). This would include, in particular, contacts that involve the neighboring W334, a residue demonstrated to be critical for TDP-43 LLPS as its mutation or deletion completely abrogates protein condensation (23). Consistent with this mechanism, the pathogenic (helix-promoting) G335D mutation and the artificial helix-enhancing mutations S333A, G333A, and G338A have all been shown to promote LLPS (47), whereas artificial mutations that break the α-helical structure of the region (e.g., A326P and M337P) have been observed to impair phase separation of the protein (15). These reports in conjunction with our own results underscore the importance of this region for the protein's LLPS and suggest that the effect of phosphorylation on TDP-43 LLPS is site specific. The differential effects of replacing Ser333 versus Gly335 with Asp can be explained by the relative α-helical propensities of the native and substituted/mutated residues in question. Like phosphoserine, Asp is less energetically favorable within the interior of α-helices than is Ser (60,61). Glycine, on the other hand, imposes the greatest energetic penalty within α-helices of all canonical amino acids, proline excepted, so mutation to any other amino acid would stabilize α-helical structure (61). When discussing this issue, it should be noted that a recent study claimed that disruption of the hydrogen bonding potential of residues within the critical A321–A329 segment by methyl-capping of backbone nitrogen atoms or glycine-mutagenesis to remove amino acid side chains inhibits TDP-43 LCD LLPS (62). Based on these data, the authors questioned the validity of the α-helical model discussed above, proposing that TDP-43 LCD LLPS is largely driven by cross-β interactions similar to those involved in amyloid fibril formation (62). However, this conclusion seems to be rather arbitrary, as capping of backbone nitrogen atoms and removal of amino acid side chains would disrupt both cross-β interactions and α-helical structure. In this same study, it was also shown that, at least under some experimental conditions, TDP-43 LCD with helix-suppressing S332G and S333G mutations forms liquid droplets similar to those of WT TDP-43 LCD. Even though this study did not provide any quantitative comparison of the LLPS propensity of these mutants and the WT protein, their finding does not appear to be fully consistent with our conclusion that the reduced LLPS propensity of the S333D phosphomimetic variant is largely due to its decreased helical propensity. To address this issue, we introduced a helix-enhancing S333A mutation within the transiently α-helical region and found that the mutation dramatically promoted TDP-43 LCD LLPS (Fig. S4). We quantified this effect by ascertaining the saturation concentrations of the S333A mutant under various conditions. The saturation concentrations of S333A TDP-43 LCD were indeed much lower than those of WT protein at all conditions tested (Fig. S4), further substantiating the relationship between the secondary structure of the transiently α-helical region and phase separation.

Another key finding of this investigation is that the S332D and S333D phosphomimetic substitutions substantially slowed TDP-43 LCD droplet aging. Although unmodified TDP-43 LCD droplets already showed significant signs of aging within 20 min of LLPS induction, droplets generated from S332D TDP-43 LCD and S333D TDP-43 LCD were completely dynamic (as indicated by essentially complete recovery of the fluorescence signal after photobleaching) up to at least 4 h post formation, and it took them as much as 24 h to transition to a highly rigid structure. As LLPS condensate aging and protein fibrillation are thought to be linked (27–29,58), we monitored the fibrillation of the proteins as well, and we found that the phosphomimetic TDP-43 variants took significantly longer to form fibrils than did WT TDP-43 LCD. This slowing of TDP-43 LCD aggregation as a result of S332D and S333D phosphomimetic substitution is consistent with cryo-EM data showing that this residue is part of the amyloid core region of the protein (11,63,64). Even though, for technical reasons, we could not selectively monitor fibrillation within the condensed phase, the correlation between the effects of the phosphomimetic substitution on the kinetics of both processes suggests that similar types of interactions are likely involved in TDP-43 LCD droplet aging and protein aggregation into amyloid fibrils. Our present finding that phosphorylation of TDP-43 at residue S332 or S333 may be a protective post-translational modification against protein aggregation is somewhat surprising, given that phosphorylation is considered a histopathological hallmark of TDP-43 proteinopathies (1,2,6,8,10,32). It should be noted, however, that the temporal relationship between TDP-43 phosphorylation and aggregation in disease is unknown, leaving open the possibility that it is the aggregated (rather than monomeric) TDP-43 that becomes phosphorylated at S333 (and possibly other sites) over time. Future work is needed to clarify this issue.

The results reported in this study were obtained using recombinant TDP-43 LCD that was phosphomimetically modified by substituting Ser332 or Ser333 with Asp. Phosphomimetic substitution is not a perfect model for this post-translational modification, as phosphate groups are bulkier and can carry larger charge. Nevertheless, this commonly used approach overcomes several technical limitations of kinase-based phosphorylation (which are especially significant in the case of intrinsically disordered proteins containing multiple phosphorylation sites), allowing preparation of a homogeneous population of protein selectively modified at a desired site. It should also be noted that studies using solely the LCD do not account for potential contributions from the N-terminal domain or the RNA recognition motifs

to TDP-43 LLPS (29), even though the LCD is the primary driver of the process (15,23,30,47), and these other domains are largely missing in the C-terminal fragments that make up disease aggregates in the brain (1,2,10). These limitations notwithstanding, our present findings provide a biophysical and mechanistically focused basis to understanding the effect of phosphorylation within the transiently α-helical region of TDP-43 LCD on protein LLPS and fibrillation. In a broader context, this study also suggests that the effects of phosphorylation on TDP-43 properties are site specific, and that phosphorylation of at least some sites does not necessarily lead to pathological consequences.

DATA AND CODE AVAILABILITY

Data can be shared upon request (contact Witold K. Surewicz at wks3@case.edu).

NMR assignments were deposited in the Biological Magnetic Resonance Bank (accession codes for WT TDP-43 LCD and S333D TDP-43 LCD are BMRB: 52253 and BMRB: 52254, respectively).

SUPPORTING MATERIAL

Supporting material can be found online at https://doi.org/10.1016/j.bpj.2024.01.001.

AUTHOR CONTRIBUTIONS

R.H., S.P., and S.B., methodology; W.K.S., project administration; R.H. and W.K.S., funding acquisition; R.H., writing – original draft; RH. and W.K.S., conceptualization; R.H. and S.B., investigation; R.H., S.P., and S.B., formal analysis; R.H. and W.K.S., writing – review and editing.

ACKNOWLEDGMENTS

We thank Krystyna Surewicz for preparing the plasmids used in this study and Matthias Buck for advice on NMR experiments and comments on the manuscript.

Funding and additional information: this work was supported in part by National Institutes of Health grants RF1 AG061797 (to W.K.S.), F30 AG071339-03 (to R.H.), T32 NS077888, and T32 GM007250. Microscopic work was supported by the National Institutes of Health Office Research Infrastructure Programs grant S10 OD024996. The content is solely the responsibility of the authors and does not necessarily represent the official views of the National Institutes of Health.

DECLARATION OF INTERESTS

The authors declare no competing interests.

REFERENCES

1. Neumann, M., D. M. Sampathu, …, V. M. Y. Lee. 2006. Ubiquitinated TDP-43 in frontotemporal lobar degeneration and amyotrophic lateral sclerosis. *Science.* 314:130–133.
2. Arai, T., M. Hasegawa, …, T. Oda. 2006. TDP-43 is a component of ubiquitin-positive tau-negative inclusions in frontotemporal lobar degeneration and amyotrophic lateral sclerosis. *Biochem. Biophys. Res. Commun.* 351:602–611.
3. Prasad, A., V. Bharathi, …, B. K. Patel. 2019. Molecular mechanisms of TDP-43 misfolding and pathology in amyotrophic lateral sclerosis. *Front. Mol. Neurosci.* 12:1–36.
4. de Boer, E. M. J., V. K. Orie, …, S. Vucic. 2020. TDP-43 proteinopathies: a new wave of neurodegenerative diseases. *J. Neurol. Neurosurg. Psychiatry.* 92:86–95.
5. Meneses, A., S. Koga, …, N. Zhao. 2021. TDP-43 Pathology in Alzheimer's Disease. *Mol. Neurodegener.* 16:1–15.
6. Neumann, M., L. K. Kwong, …, V. M. Y. Lee. 2009. Phosphorylation of S409/410 of TDP-43 is a consistent feature in all sporadic and familial forms of TDP-43 proteinopathies. *Acta Neuropathol.* 117:137–149.
7. Nonaka, T., F. Kametani, …, M. Hasegawa. 2009. Truncation and pathogenic mutations facilitate the formation of intracellular aggregates of TDP-43. *Hum. Mol. Genet.* 18:3353–3364.
8. Hasegawa, M., T. Arai, …, H. Akiyama. 2008. Phosphorylated TDP-43 in frontotemporal lobar degeneration and amyotrophic lateral sclerosis. *Ann. Neurol.* 64:60–70.
9. François-Moutal, L., S. Perez-Miller, …, M. Khanna. 2019. Structural Insights Into TDP-43 and Effects of Post-translational Modifications. *Front. Mol. Neurosci.* 12:301.
10. Igaz, L. M., L. K. Kwong, …, V. M. Y. Lee. 2008. Enrichment of C-terminal fragments in TAR DNA-binding protein-43 cytoplasmic inclusions in brain but not in spinal cord of frontotemporal lobar degeneration and amyotrophic lateral sclerosis. *Am. J. Pathol.* 173:182–194.
11. Arseni, D., M. Hasegawa, …, B. Ryskeldi-falcon. 2022. Structure of pathological TDP-43 filaments from ALS with FTLD. *Nature.* 601:139–143.
12. Johnson, B. S., D. Snead, …, A. D. Gitler. 2009. TDP-43 is intrinsically aggregation-prone, and amyotrophic lateral sclerosis-linked mutations accelerate aggregation and increase toxicity. *J. Biol. Chem.* 284:20329–20339.
13. Furukawa, Y., K. Kaneko, …, N. Nukina. 2011. A Seeding Reaction Recapitulates Intracellular Formation of Sarkosyl-insoluble Transactivation Response Element (TAR) DNA-binding Protein-43 Inclusions. *J. Biol. Chem.* 286:18664–18672.
14. Buratti, E. 2015. Functional Significance of TDP-43 Mutations in Disease. *In* Advances in Genetics. T. Friedmann, J. C. Dunlap, and S. F. Goodwin, eds Academic Press, pp. 1–53.
15. Conicella, A. E., G. H. Zerze, …, N. L. Fawzi. 2016. ALS Mutations Disrupt Phase Separation Mediated by α-Helical Structure in the TDP-43 Low-Complexity C-Terminal Domain. *Structure.* 24:1537–1549.
16. Schmidt, H. B., and R. Rohatgi. 2016. In vivo formation of vacuolated multi-phase compartments lacking membranes. *Cell Rep.* 16:1228–1236.
17. Carey, J. L., and L. Guo. 2022. Liquid-Liquid Phase Separation of TDP-43 and FUS in Physiology and Pathology of Neurodegenerative Diseases. *Front. Mol. Biosci.* 9:826719–826720.
18. Banani, S. F., H. O. Lee, …, M. K. Rosen. 2017. Biomolecular condensates: Organizers of cellular biochemistry. *Nat. Rev. Mol. Cell Biol.* 18:285–298.
19. Shin, Y., and C. P. Brangwynne. 2017. Liquid phase condensation in cell physiology and disease. *Science.* 357, eaaf4382.
20. Alberti, S., and D. Dormann. 2019. Liquid – Liquid Phase Separation in Disease. *Annu. Rev. Genet.* 53:171–194.
21. Li, H. R., T. C. Chen, …, J. r. Huang. 2018. The physical forces mediating self-association and phase-separation in the C-terminal domain of TDP-43. *BBA - Proteins Proteomics.* 1866:214–223.
22. Jiang, L. L., M. X. Che, …, H. Y. Hu. 2013. Structural transformation of the amyloidogenic core region of TDP-43 protein initiates its aggregation and cytoplasmic inclusion. *J. Biol. Chem.* 288:19614–19624.

23. Li, H. R., W. C. Chiang, …, J. R. Huang. 2018. TAR DNA-binding protein 43 (TDP-43) liquid-liquid phase separation is mediated by just a few aromatic residues. *J. Biol. Chem.* 293:6090–6098.
24. Schmidt, H. B., A. Barreau, and R. Rohatgi. 2019. Phase separation-deficient TDP43 remains functional in splicing. *Nat. Commun.* 10:4890.
25. Feng, Z., X. Chen, …, M. Zhang. 2019. Formation of biological condensates via phase separation: Characteristic , analytical methods, and physiological implications. *J. Biol. Chem.* 294:14823–14835.
26. Wang, B., L. Zhang, …, F. Zhou. 2021. Liquid – liquid phase separation in human health and diseases. *Signal Transduct. Targeted Ther.* 6:290.
27. Babinchak, W. M., and W. K. Surewicz. 2020. Liquid–Liquid Phase Separation and Its Mechanistic Role in Pathological Protein Aggregation. *J. Mol. Biol.* 432:1910–1925.
28. Zbinden, A., M. Pérez-Berlanga, …, M. Polymenidou. 2020. Phase Separation and Neurodegenerative Diseases: A Disturbance in the Force. *Dev. Cell.* 55:45–68.
29. Haider, R., S. Boyko, and W. K. Surewicz. 2022. Liquid-liquid phase separation in neurodegenerative diseases. *In* Droplets of Life: Membrane-Less Organelles, Biomolecular Condensates, and Biological Liquid-Liquid Phase Separation, 1st Ed. V. Uversky, ed Academic Press, pp. 619–650.
30. Babinchak, W. M., R. Haider, …, W. K. Surewicz. 2019. The role of liquid-liquid phase separation in aggregation of the TDP-43 low-complexity domain. *J. Biol. Chem.* 294:6306–6317.
31. Babinchak, W. M., B. K. Dumm, …, W. K. Surewicz. 2020. Small molecules as potent biphasic modulators of protein liquid-liquid phase separation. *Nat. Commun.* 11:5574.
32. Kametani, F., T. Obi, …, M. Hasegawa. 2016. Mass spectrometric analysis of accumulated TDP-43 in amyotrophic lateral sclerosis brains. *Sci. Rep.* 6, 23281.
33. Neumann, M., P. Frick, …, I. R. Mackenzie. 2021. Correction to: Antibody against TDP-43 phosphorylated at serine 369 suggests conformational differences of TDP-43 aggregates among FTLD-TDP subtypes. *Acta Neuropathol.* 141:137.
34. Eck, R. J., B. C. Kraemer, and N. F. Liachko. 2021. Regulation of TDP-43 phosphorylation in aging and disease. *GeroScience.* 43:1605–1614.
35. Gruijs da Silva, L. A., F. Simonetti, …, D. Dormann. 2022. Disease-linked TDP-43 hyperphosphorylation suppresses TDP-43 condensation and aggregation. *EMBO J.* 41, e108443.
36. Wang, A., A. E. Conicella, …, N. L. Fawzi. 2018. A single N-terminal phosphomimic disrupts TDP-43 polymerization, phase separation, and RNA splicing. *EMBO J.* 37, e97452.
37. Delaglio, F., S. Grzesiek, …, A. Bax. 1995. NMRPipe: a multidimensional spectral processing system based on UNIX pipes. *J. Biomol. NMR.* 6:277–293.
38. Ying, J., F. Delaglio, …, A. Bax. 2017. Sparse multidimensional iterative lineshape-enhanced (SMILE) reconstruction of both non-uniformly sampled and conventional NMR data. *J. Biomol. NMR.* 68:101–118.
39. Lee, W., M. Tonelli, and J. L. Markley. 2015. NMRFAM-SPARKY: enhanced software for biomolecular NMR spectroscopy. *Bioinformatics.* 31:1325–1327.
40. Grzesiek, S., and A. D. Bax. 1992. Improved 3D triple-resonance NMR techniques applied to a 31 kDa protein. *J. Magn. Reson.* 96:432–440.
41. Schleucher, J., M. Sattler, and C. Griesinger. 1993. Coherence Selection by Gradients without Signal Attenuation: Application to the Three-Dimensional HNCO Experiment. *Angew. Chem.* 32:1489–1491.
42. Kay, L. E., G. Y. Xu, and T. Yamazaki. 1994. Enhanced-Sensitivity Triple-Resonance Spectroscopy with Minimal H2O Saturation. *J. Magn. Reson.* 109:129–133.
43. Schanda, P., H. Van Melckebeke, and B. Brutscher. 2006. Speeding up three-dimensional protein NMR experiments to a few minutes. *J. Am. Chem. Soc.* 128:9042–9043.
44. Lescop, E., P. Schanda, and B. Brutscher. 2007. A set of BEST triple-resonance experiments for time-optimized protein resonance assignment. *J. Magn. Reson.* 187:163–169.
45. Grzesiek, S., and A. Bax. 1993. Amino acid type determination in the sequential assignment procedure of uniformly 13C/15N-enriched proteins. *J. Biomol. NMR.* 3:185–204.
46. Muhandiram, D. R., and L. E. Kay. 1994. Gradient-Enhanced Triple-Resonance Three-Dimensional NMR Experiments with Improved Sensitivity. *J. Magn. Reson. B.* 103:203–216.
47. Conicella, A. E., G. L. Dignon, …, N. L. Fawzi. 2020. TDP-43 α-helical structure tunes liquid-liquid phase separation and function. *Proc. Natl. Acad. Sci. USA.* 117:5883–5894.
48. Lim, L., Y. Wei, …, J. Song. 2016. ALS-Causing Mutations Significantly Perturb the Self-Assembly and Interaction with Nucleic Acid of the Intrinsically Disordered Prion-Like Domain of TDP-43. *PLoS Biol.* 14, e1002338.
49. Maltsev, A., and F. Poulsen. 2019. Poulsen IDP/IUP random coil chemical shifts. [online]. https://spin.niddk.nih.gov/bax/nmrserver/Poulsen_rc_CS/.
50. Kjaergaard, M., S. Brander, and F. M. Poulsen. 2011. Random coil chemical shift for intrinsically disordered proteins: effects of temperature and pH. *J. Biomol. NMR.* 49:139–149.
51. Nonaka, T., G. Suzuki, …, M. Hasegawa. 2016. Phosphorylation of TAR DNA-binding protein of 43 kDa (TDP-43) by truncated casein kinase 1δ triggers mislocalization and accumulation of TDP-43. *J. Biol. Chem.* 291:5473–5483.
52. Murthy, A. C., and N. L. Fawzi. 2020. The (un)structural biology of biomolecular liquid-liquid phase separation using NMR spectroscopy. *J. Biol. Chem.* 295:2375–2384.
53. Wishart, D. S., and B. D. Sykes. 1994. The 13C Chemical-Shift Index: A simple method for the identification of protein secondary structure using 13C chemical-shift data. *J. Biomol. NMR.* 4:171–180.
54. Jo, Y., J. Jang, …, Y. Jung. 2022. Determinants for intrinsically disordered protein recruitment into phase-separated protein condensates. *Chem. Sci.* 13:522–530.
55. Kamagata, K., N. Iwaki, …, Y. Levy. 2021. Molecular principles of recruitment and dynamics of guest proteins in liquid droplets. *Sci. Rep.* 11, 19323.
56. Kamagata, K., N. Iwaki, …, S. Sakomoto. 2022. Structure - dependent recruitment and diffusion of guest proteins in liquid droplets of FUS. *Sci. Rep.* 12:7101.
57. Han, T. W., M. Kato, …, S. L. McKnight. 2012. Cell-free formation of RNA granules: bound RNAs identify features and components of cellular assemblies. *Cell.* 149:768–779.
58. Lin, Y., D. S. W. Protter, …, R. Parker. 2015. Formation and Maturation of Phase Separated Liquid Droplets by RNA Binding Proteins. *Mol. Cell.* 60:208–219.
59. Ryan, V. H., and N. L. Fawzi. 2019. Physiological, pathological, and targetable membraneless organelles in neurons. *Trends Neurosci.* 42:693–708.
60. Andrew, C. D., J. Warwicker, …, A. J. Doig. 2002. Effect of phosphorylation on alpha-helix stability as a function of position. *Biochemistry.* 41:1897–1905.
61. Pace, C. N., and J. M. Scholtz. 1998. A helix propensity scale based on experimental studies of peptides and proteins. *Biophys. J.* 75:422–427.
62. Zhou, X., L. Sumrow, …, S. L. McKnight. 2022. Mutations linked to neurological disease enhance self-association of low-complexity protein sequences. *Science.* 377:eabn5582.
63. Li, Q., W. M. Babinchak, and W. K. Surewicz. 2021. Cryo-EM structure of amyloid fibrils formed by the entire low complexity domain of TDP-43. *Nat. Commun.* 12:1620.
64. Cao, Q., D. R. Boyer, …, D. S. Eisenberg. 2019. Cryo-EM structures of four polymorphic TDP-43 amyloid cores. *Nat. Struct. Mol. Biol.* 26:619–627.